Chapter 2

Formation of Porous Carbon Materials with in Situ Generated NaF Nanotemplate

2.1 Introduction

Porous materials provides excellent opportunities in numerous technological applications.[1,2] Among different types of porous materials, porous carbon (p-C) has high potentials as the component in catalysis, adsorption, sensing and fuel-cell systems.[3-6] Many types of carbon materials with different pore sizes have been fabricated through replica approaches employing various zeolite or silica as the templates and casts.[7-12] Another frequently used method employs defluorination of PTFE, poly(tetrafluoroethylene), by alkali metals.[13-15] In the present work, we wish to report an efficient new synthesis of p-C by reacting the vapor of C_6F_6 with Na metal. The growth is an interesting example of a phase separation assisted self-templating process. Moreover, template-assisted growth of carbon nanotubes (CNT) has been demonstrated to be an efficient method to produce aligned arrays of CNT.[16-23] by coupling the reaction between C_6F_6 and Na with a reactive–template strategy reported previously,[24] which employs anodic aluminum oxide (AAO) membrane filled with Na metal as an active cast, arrays of porous CNT (p-CNT) can be fabricated.

2.2 Experimental Section

2.2.1 Synthesis of p-C

Na metal was prepared by pyrolyzing NaH (0.15 g, 6.3 mmol, Aldrich) under Ar atmosphere on a silica boat inside a tube furnace at 623 K for 1 h. To the as-formed Na metal at 623 K, C_6F_6 (99 %, Aldrich) vaporized at 298 K was introduced by bubbling under

a constant flow of Ar (5 sccm) for 4 h. The as-prepared black product was further washed in refluxing distilled water (300 mL) overnight. The solid product was collected, rinsed with distilled water, and dried at 373 K in air.

2.2.2 Synthesis of p-CNT

Na@AAO was prepared by pyrolyzing of NaH (0.15 g, 6.3 mmol, Aldrich) on AAO (Whatman Anodisc 13, pore diameter of 200 nm, thickness of 60 μm) at 623 K for 1 h under an Ar atmosphere.[24] The as-prepared Na@AAO was reacted with C_6F_6 (99 %, Aldrich), maintained at 298 K and bubbled under the assistance of a constant flow of Ar (5 sccm), at 323 and 623 K for 4 h to generate black products. The as-prepared products were further washed in refluxing distilled water (300 mL) overnight. Then, the AAO was removed by immersion in 48 % HF at room temperature for 9 h. Finally, the products were filtered, rinsed with distilled water and dried at 373 K in air.

2.2.3 Characterization of p-C materials

A scanning electron microscope (SEM, JEOL JSM-6330F at 15 kV and HITACHI S-4000 at 25 kV) and a high-resolution transmission electron microscope (HRTEM, JEOL JEM-4000 at 400 kV) were used to observe the sample morphology. Energy dispersive X-ray spectroscopy (EDS) was used to confirm the element composition of the samples. Crystallinity of the samples was investigated by an X-ray diffractometer (XRD, BRUKER AXS D8 ADVANCE, Cu K_α radiation, 40 kV and 40 mA). A Brunauer-Emmett-Teller instrument (BET, Micromeritics ASAP 2010, at 77 K using N_2 gas) was used to investigate surface area and pore size distribution of the samples. Thermal gravimetric analysis (TGA) was carried out on a Pyris Diamond TG/DTA instrument (heating rate of 5 deg/min from room temperature to 1173 K, air flow rate at 100 mL/min.

2.3 Results

2.3.1 Preparation and characterization of p-C

In general, via a Wurtz type coupling reaction,[25] the vapor of C_6F_6 was reacted with Na metal, prepared by pyrolyzing NaH under Ar, at 623 K for 1 h to offer a dark solid product. As described in the next section, the reaction can be performed at a temperature as low as 323 K. As shown in Figure 2.1, XRD of the solid produced at 323 K and 623 K displays a diffraction pattern that is composed of a broad (002) reflection from graphite (JCPDS 23-0064) and (200), (220) and (222) reflections from NaF (JCPDS 36-1455). No other significant structural information was observed. After the sample was washed with distilled water, the salt was removed and the black solid product was collected.

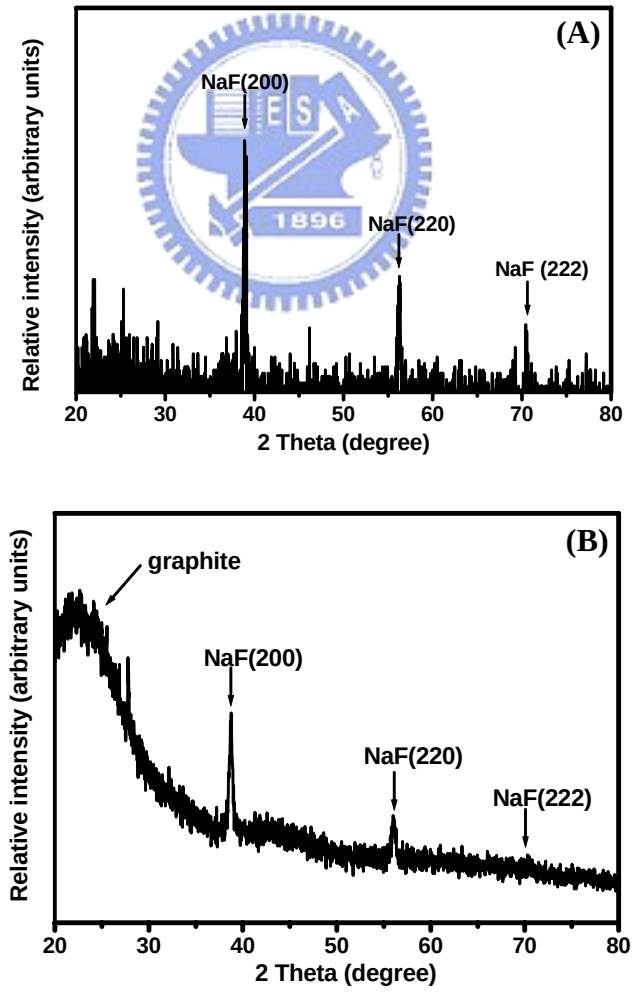

Figure 2.1 XRD of an as-formed raw product prepared at (A) 323 K; (B) 623 K.

Figure 2.2A is a typical scanning electron microscopic (SEM) image of the isolated material. In the enlarged image, Figure 2.2B, morphology of the material is shown to have innumerable pores with diameters less than 200 nm. X-ray energy dispersive spectroscopy (EDX) confirms that the solid is composed of carbon while the concentrations of sodium and fluorine are below the detection limits. A low-magnification transmission electron microscopic (TEM) image in Figure 2.2C also shows the porous nature of the solid product, with pore diameters less than 200 nm. In a high-resolution transmission electron microscopic (HRTEM) image (Figure 2.2D) of the sample, the presence of fringes spaced ca. 0.35 nm apart is observed. Since the fringes are not well ordered, we suggest that the edges of the p-C have a short-range ordering of graphite texture. The thickness of the p-C wall, deduced from the image, is 3 - 15 nm.

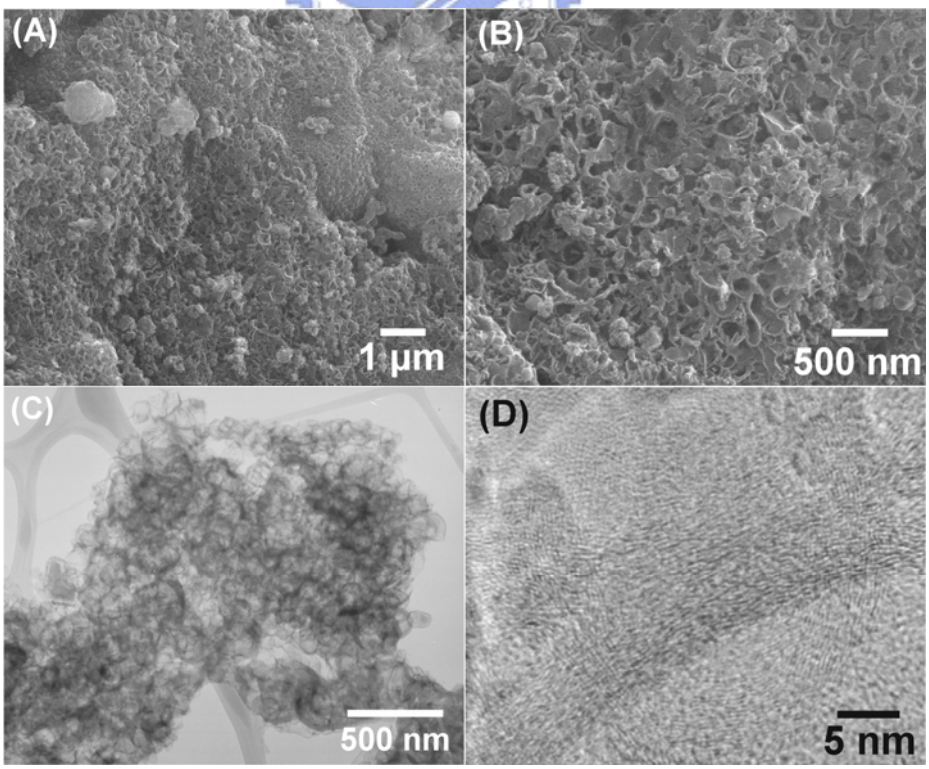

Figure 2.2 Images of p-C prepared at 623 K. (A) Low and (B) high magnification SEM; (C) low magnification and (D) high resolution TEM.

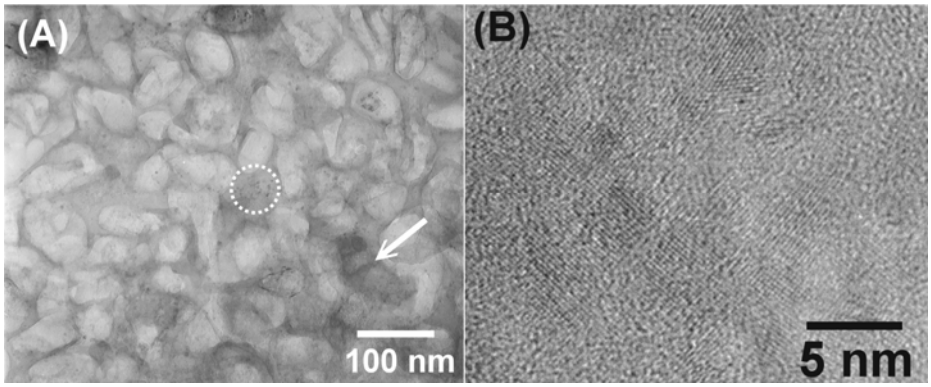

Figure 2.3 TEM images of phase separated p-C and NaF. (A) Low magnification image showing NaF crystals pointed by the arrow and (B) high resolution image of NaF nanocrystals selected from the circled area in (A).

Occasionally, NaF nanoparticles can be observed inside p-C by TEM. For example, at point indicated by the arrow in Figure 2.3A, the presence of a NaF crystal ca. 80 nm in size is identified by EDS. In addition, from the circled area in Figure 2.3A, several minute nanocrystals with sizes of 2 - 4 nm are observed by HRTEM, as shown in Figure 2.3B. The lattice fringes are spaced 0.23 nm apart, which coincides well with the {200} interplanar distance of NaF (JCPDS 36-1455). This confirms that the nanosized NaF crystals acted as the templates for the formation of the porous structure.

2.3.2 Preparation and characterization of p-CNT

Previously, we demonstrated that by pyrolyzing NaH on top of AAO membranes, the as-formed Na flowed into the channels of AAO and produced reactive templates Na@AAO.[24] By reacting Na@AAO with C_6Cl_6, amorphous carbon nanotubes were fabricated inside the AAO cast. On the basis of the product morphology, we concluded that metallic Na existed as nanotubes inside the AAO channels of Na@AAO. We extend the strategy in this study. By employing C_6F_6 to react with Na@AAO at 323 and 623 K, black products were insolated. After the AAO template and the salt were removed, the products were investigated by electron microscopy. A low magnification SEM image of the product prepared at 323 K after the AAO cast was removed is shown in Figure 2.4A. It displays that

the sample is an aligned array of nanotubes with diameters of 200 - 250 nm. This is close to the channel diameter of the AAO template. An EDS study confirms that the material is composed of carbon. From other SEM images, the length of the nanotubes is estimated to be 60 μm, which is close to the thickness of the AAO membrane. Figure 2.4B shows an enlarged SEM image of a p-CNT with undulate inner and outer surfaces. On the basis of the results discussed in the previous section, the unevenness of the surfaces is attributed to the presence of pores generated by the byproduct NaF. A TEM image (Figure 2.4C) of a tube also shows an average diameter of 220 nm, which is comparable to the SEM observation. In Figure 2.4D, an HRTEM image shows the detailed microstructure of a p-CNT. It reveals a wall thickness of ca. 15 – 20 nm and numerous pores of several nanometers inside the wall. Thus, we successfully fabricated, via a simple process, a new type of p-CNT from this unique self-templating and casting approach.

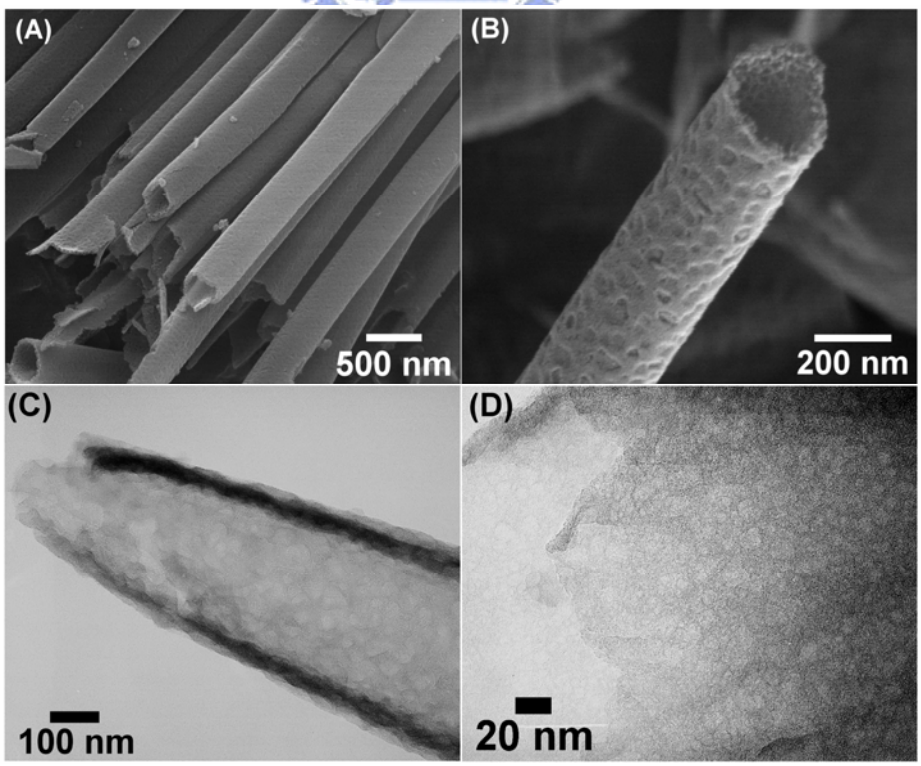

Figure 2.4 Images of p-CNT prepared at 323 K. (A) Low and (B) high magnification SEM; (C) low and (D) high resolution TEM.

From SEM images and EDS studies, the sample prepared at 623 K is also identified to be an aligned array of p-CNT (lengths of ca. 60 μm, diameters of ca. 200 – 300 nm, and pore sizes of ca. 20 - 100 nm). Examples of low- and high-magnification images are shown in Figure 2.5, panels A and B, respectively. In Figure 2.5C, a TEM image of an individual p-CNT shows the presence of innumerable pores of 15 - 90 nm in the wall, which correlates well with the SEM observation. An HRTEM image (Figure 2.5D), selected from the edge of the p-CNT shown in Figure 2.5C, displays textured graphene layers. The overall pore structure in p-CNT is nearly identical with that of p-C discussed above. A TGA result (Figure 2.6) showed that a p-CNT sample, annealed at 1173 K under vacuum followed by removing the AAO template, was oxidized in air at 710 K. The sharp weight loss suggests that the sample contained less ordered carbon structure.[26] The process removed ca. 63% weight of the material in the sample. The residue, which was stable up to 1173 K, is assigned to unremoved NaF byproduct.

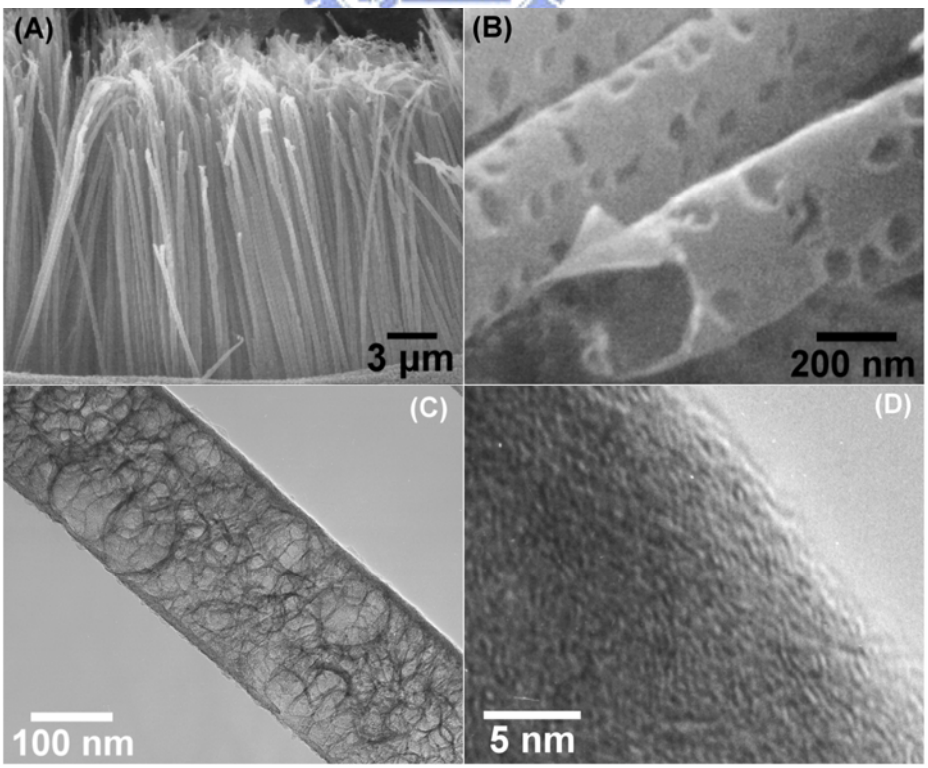

Figure 2.5 Images of p-CNT prepared at 623 K. (A) Low and (B) high magnification SEM; (C) low and (D) high resolution TEM.

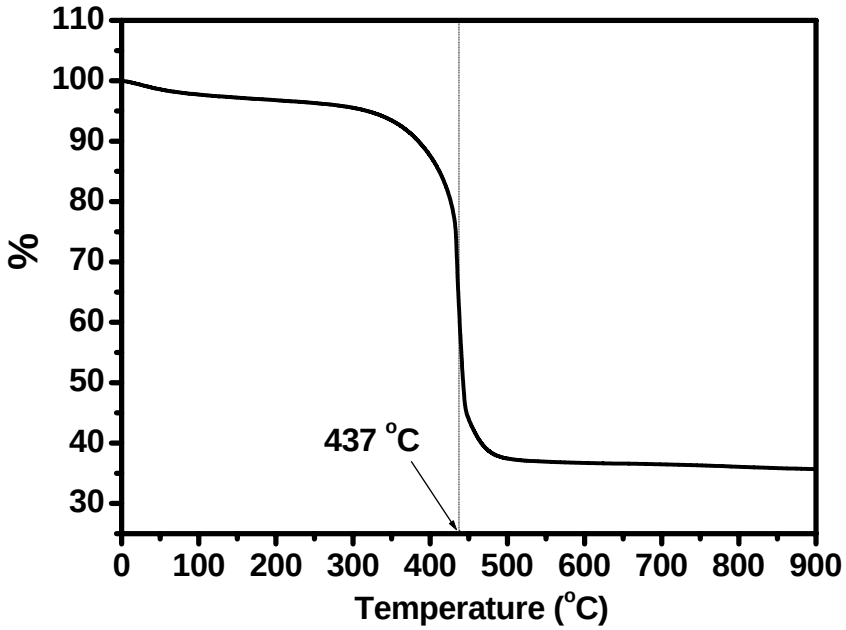

Figure 2.6 TGA (heating rate: 5 deg/min from 298 K to 1173 K, air flow rate: 100 mL/min) of p-CNT prepared at 623 K and annealed at 1173 K under low pressure $1*10^{-3}$ torr. Significant weight loss occurred at 710 K due to oxidation of the carbon. The residual weight is assigned to the unremoved NaF byproduct.

The following observation further support the role of the NaF byproduct as an in-situ generated nanotemplate for pore formation. Figure 2.7A shows an enlarged cross-sectional SEM view of an AAO membrane after p-CNT formed at 623 K was removed from the cast. On the exposed channel surface, solid islands with sizes of several tens nanometers are observed. An EDS study (Figure 2.7B) of an island, selected from the circled area in Figure 2.7A, reveals the presence of Na and F. Consequently, the islands are identified to be NaF crystals. The crystal size and shape are in good agreement with the pore structures observed in Figure 2.5B and 2.5C. Thus, we conclude that the NaF nanocrystals and the AAO membrane acted as the cast to influence the p-CNT structure cooperatively. The NaF worked as the in-situ generated nanotemplate, which assisted the pore formation, while the AAO membrane performed the role of the cast, which aided the tubular shape development.

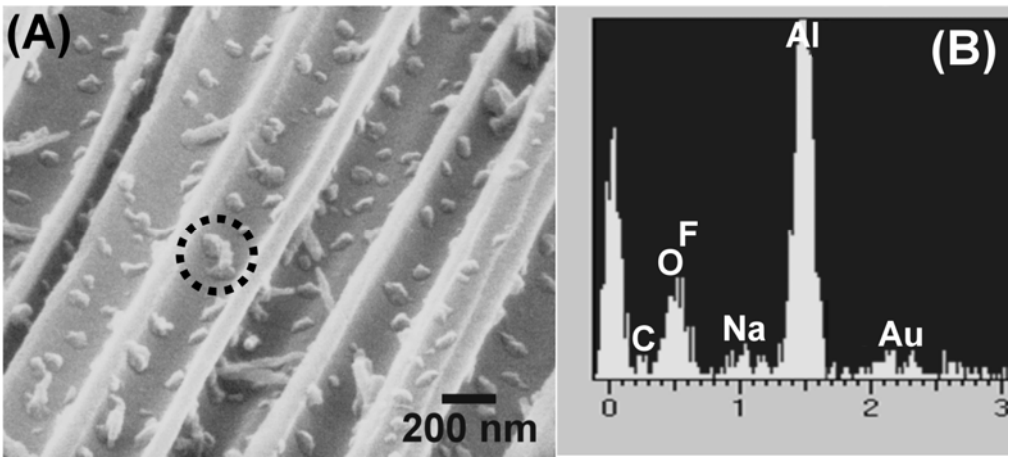

Figure 2.7 (A) Cross sectional SEM image of AAO after removal of p-CNT prepared at 623 K showing crystals in the channels. (B) EDS from the circled area in (A).

2.3.3 BET analysis of p-C materials prepared at 623 K

From the SEM and TEM studies discussed above, the carbon materials possessed pores with sizes ranging from several to several tens of nanometers. Typical nitrogen adsorption-desorption isotherms of p-C and p-CNT prepared at 623 K are shown in Figure 2.8, panels A and B, respectively. In the region of middle and high P/P_o, the amount of N_2 adsorption increases sharply. The phenomenon, a steep increase in the isotherm at high pressures ($P/P_o \rightarrow 1$), confirms that large macropores are present in the materials. In addition, large hystereses are observed in Figure 2.8. This is evidence for a network pore system with distinct polydispersity in sizes.[27,28] The observation is in good agreement with the TEM images in Figures 2.2C and 2.5C. Estimated from Figure 2.8A, the Brunauer-Emmett-Teller (BET) surface area is 161 m^2g^{-1}. By using Barret-Joyner-Halenda (BJH) method, the smallest pore size in p-C can be calculated from the desorption branch of the nitrogen isotherm. The reason desorption branches, instead of the adsorption ones, were used is explained below. According to the Kelvin equation,[27] the desorption branch of the isotherms is usually more reasonable to derive the diameters of cylindrical pores when the contact angle between the adsorbate, which was nitrogen in this study, and the pore wall is assumed to be zero. Nevertheless, the huge hysteresis loops of the isotherms of p-C and

p-CNT materials indicate the pores could probably be described by an ink-bottle model.[27] The rapid increase in adsorption volume in the adsorption branches at higher P/P_0 was related to the large diameter of the bottle shaped pores. While that in the desorption branches at lower P/P_0 was correlated to the smaller diameter of the neck. Thus, the pores of this region are estimated to be as small as 3 - 3.5 nm. This agrees with the mesopores (sizes 2 - 4 nm) observed in Figure 2.3B, which formed after the NaF nanocrystals in the carbon matrix were removed. This is comparable to a previous study in which, removal of fluorides from a carbon matrix by acid treatment was found to leave empty sites as pores.[29] The BET surface area estimated from Figure 2.8B is 183 m^2g^{-1}. The calculated pore size distribution from the desorption branch, using the BJH method, also displays that the pores exhibit a size limit at 3 - 3.5 nm. These experimental data are comparable to the values reported recently in another study.[11]

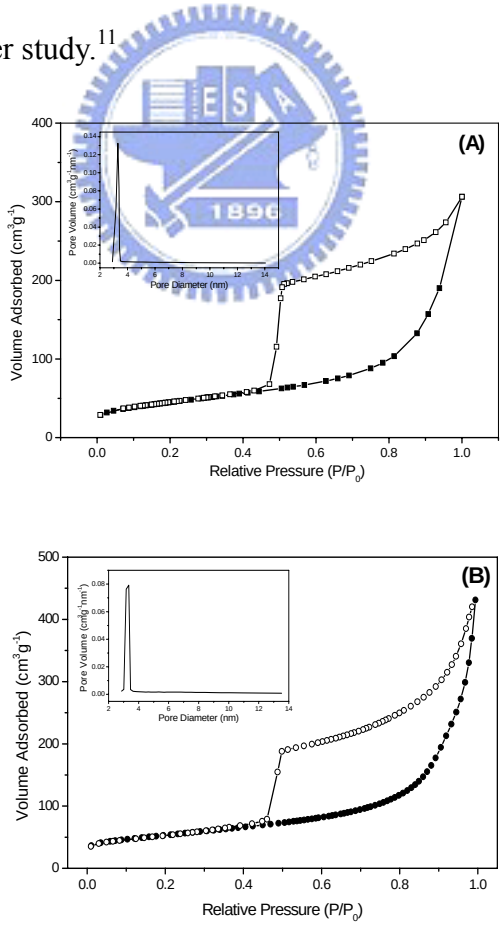

Figure 2.8 Nitrogen adsorption-desorption isotherms and BJH pore size distribution from the desorption branches (insets). (A) p-C (■: adsorption branch; □: desorption branch) and (B) p-CNT (●: adsorption branch; ○: desorption branch).

2.3.4 Graphitzed of p-CNTs at 3073 K

The p-CNTs were graphitized further at 3073 K for 0.5 h. Figure 2.9A is a SEM image of as-graphitized p-CNTs shown good uniformity and porous-like structure (Figure 2.9B). These graphitized p-CNTs have diameter of less than 300 nm, the same as the as-growth p-CNTs prepared at 623 K. In Figure 2.9C, the TEM image of a graphitized p-CNT is shown. While the porous wall structure is essentially preserved, Figure 2.9D shows an enlarged view of pores from a circled area in Figure 2.9C. In Figure 2.9E, an HRTEM image of a boxed area selected from Figure 2.9C shows the crystallinity of the carbon layers is increased and the structure of a section of the p-CNT wall with a thickness of 12.6 nm, which equals the thickness of forty graphene layers.

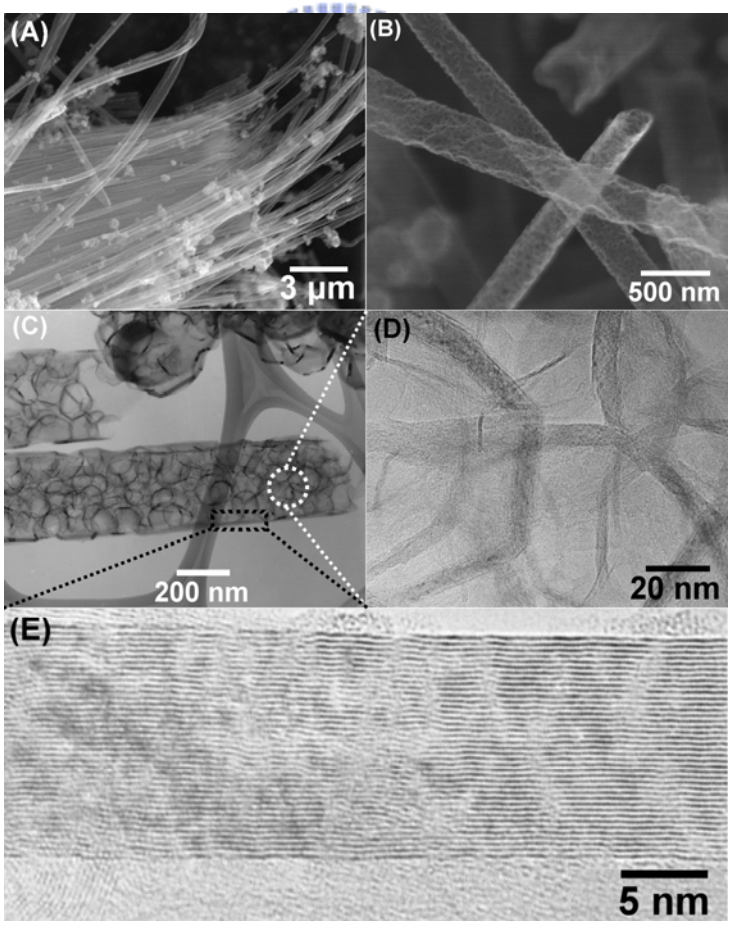

Figure 2.9 SEM images of (A) low and (B) high magnifications of graphitized p-CNT; (C) TEM images of graphitized-p-CNT (D) Zoom-in TEM image of the circle area in figure 2.9C. (E) HRTEM image gotten from the boxed area in figure 2.9C graphitized at 3073 K.

The Raman spectrum was used to characterize the graphitized p-CNTs and similar to previously reported. Figure 2.10 compared the Raman spectra measured from p-CNTs grown at 623 K (bottom) and graphitized at 3073 K (upper). In the Figure 2.10 (bottom), G-band at 1592 cm^{-1} is close to E_{2g} mode of graphite and is associated with the vibration mode of sp^2-bonded carbon atoms in the two-dimentional hexagonal lattice. D-band at 1354 cm^{-1} is associated with the vibration of carbon atoms with dangling bond in the plane terminations of disordered graphite. In the Figure 2.10 (upper), the graphitized CNTs shown G-band at 1575 cm^{-1} and D-band at 1349 cm^{-1}. The I_D/I_G intensity ratio beetween D band and G band can be used to estimated the graphitic ordering and conbined with La (La = $44(I_D/I_G)^{-1}$), which in our case is related to the length of graphitic layer. The p-CNTs prepared at 623 K shown La = 1.8 nm. The graphitized p-CNTs have obviously ordering graphitic layer improvement got La = 26.5 nm.

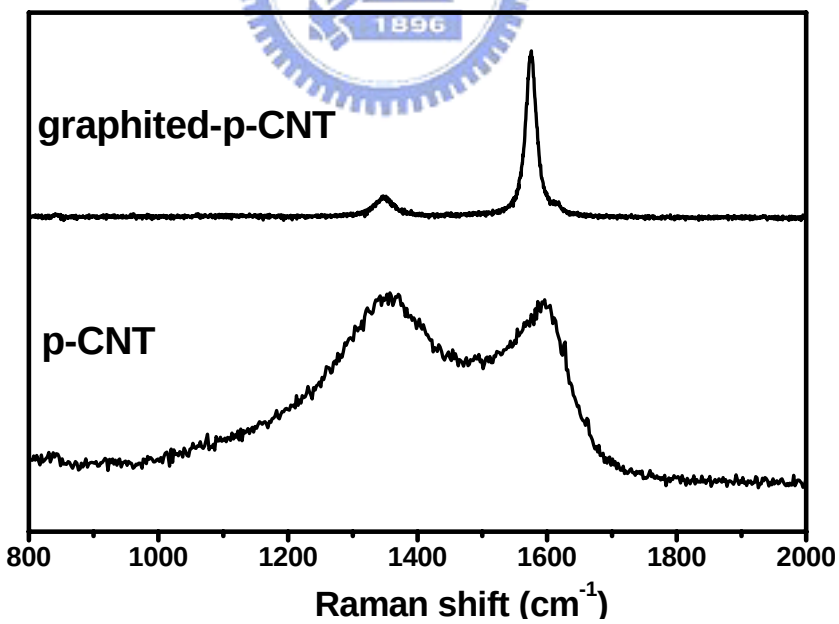

Figure 2.10 Raman spectra of p-CNT (lower) prepared at 623 K and graphited-p-CNT (upper) graphited at 3073 K.

2.4. Discussion

For summary, a scheme for the formation of p-C materials by reacting C_6F_6 with Na and Na@AAO is shown in Scheme 2.1. The process utilized the strong reducing capability of metallic Na to remove F atoms from C_6F_6 and facilitated the solid carbon formation via a Wurtz-type coupling reaction. As shown in the TEM images in Figure 2.3, due to phase separation, the byproduct NaF of various sizes are incorporated within the carbon solid. This assists the formation of the macro and the mesoporous structures. Another possible origin of the mesopores, as suggested in the literature, is from the disordered stacking of graphene sheets shown in Figures 2.2D and 2.5D.[30] The p-CNT prepared from C_6F_6 in this study shows significant structural difference from the CNT, which had smooth nonporous walls, synthesized from C_6Cl_6 previously.[24] The origin of this is proposed to be the difference in physical properties of the byproduct salts NaF and NaCl. This includes the melting point and the energy of formation, which would affect the crystal sizes and their affinity to surroundings. In this study, as shown in Figures 2.3 and 2.6, we find that NaF adhere better to the AAO template and the as-formed carbon solid.[31] This was not observed in the previous investigation employing C_6Cl_6 as the source of carbon.[24]

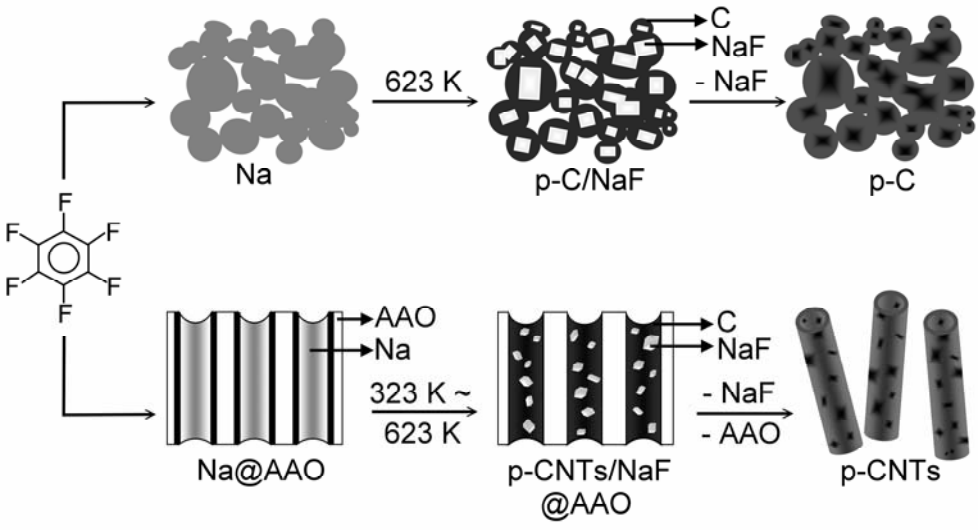

Scheme 2.1 The Preparations of p-C and p-CNT.

It is striking to discover that p-CNT can be formed at a temperature as low as 323 K. This observation may be attributed to the high energy of formation of NaF and the highly exothermic reaction.[31] The reaction rate probably is accelerated significantly within nanoscopic zones where the reaction between gaseous C_6F_6 molecules and Na releases enough energy to overcome the overall reaction barrier.

2.5. Conclusions

By employing C_6F_6 to react with Na, a unique type of p-C material was formed. The self-generated NaF acted as the nanotemplate to shape the carbon material into the observed porous structure. By using the reactive template Na@AAO, the p-C can be fabricated further into nanotubes with a structure significantly different from the Iijima type CNT.[32,33] The process reported here is relatively low temperature and does not require plasma, autoclave and catalyst assistance. We anticipate these new materials to be useful in many applications. For example, a preliminary investigation showed that p-CNT retained essential nanostructural features after being graphitized at 3073 K. We expect polymer chains could entangle this unique carbon material effectively by passing through the porous structure.[34,35] This may offer a new type of low-density and high strength composite material. Investigation is in progress.

References

(1) Ying, J. Y.; Mehnert, C. P.; Wong, M. S. *Angew. Chem., Int. Ed. Engl.* **1999**, *38*, 56.

(2) Schüth, F. *Angew. Chem., Int. Ed.* **2003**, *42*, 3604.

(3) Che, G.; Lakshmi, B. B.; Fisher, E. R.; Martin, C. R. *Nature* **1998**, *393*, 346.

(4) Joo, S. H.; Choi, S. J.; Oh, I.; Kwak, J.; Liu, Z.; Terasaki, O.; Ryoo, R. *Nature* **2001**, *412*, 169.

(5) Dalton, A. B.; Collins, S.; Munoz, E.; Razal, J. M.; Ebron, V. H.; Ferratis, J. P.; Coleman, J. N.; Kim, B. G.; Baughman, R. H. *Nature* **2003**, *423*, 703.

(6) Sakintuna, B.; Yurum, Y. *Ind. Eng. Chem. Res.* **2005**, *44*, 2893.

(7) Kyotani, T.; Nagai, T.; Inoue, S.; Tomita, A. *Chem. Mater.* **1997**, *9*, 609.

(8) Johnson, S. A.; Brigham, E. S.; Ollivier, P. J.; Mallouk, T. E. *Chem. Mater.* **1997**, *9*, 2448.

(9) Lee, J.; Yoon, S.; Hyeon, T.; Oh, S. M.; Kim, K. B. *Chem. Commun.* **1999**, 2177.

(10) Ryoo, R.; Joo, S. H.; Kruk, M.; Jaroniec, M. *Adv. Mater.* **2001**, *13*, 677.

(11) Kim, M.; Sohn, K.; Kim, J.; Hyeon, T. *Chem. Commun.* **2003**, 652.

(12) Han, B. H.; Zhou, W.; Sayari, A. *J. Am. Chem. Soc.* **2003**, *125*, 3444.

(13) Tanaike, O.; Hatori, H.; Yamada, Y.; Shiraishi, S.; Oya, A. *Carbon* **2003**, *41*, 1759.

(14) Tanaike, O.; Yoshizawa, N.; Hatori, H.; Yamada, Y.; Shiraishi, S.; Oya, A. *Carbon* **2002**, *40*, 457.

(15) Hlavaty, J.; Havan, L. *Carbon* **1999**, *37*, 1029.

(16) Miao, J. Y.; Cai, Y.; Chan, Y. F.; Sheng, P.; Wang, N. *J. Phys. Chem. B* **2006**, *110*, 2080.

(17) Sui, Y. C.; Acosta, D. R.; Gonzalez-Leon, J. A.; Bermudez, A.; Feuchtwanger, J. Cui, B. Z.; Flores, J. O.; Saniger, J. M. *J. Phys. Chem. B* **2001**, *105*, 1523.

(18) Rajesh, B.; Thampi, K. R.; Bonard, J. M.; Xanthopoulos, N.; Mathieu, H. J.; Viswanathan, B. *J. Phys. Chem. B* **2003**, *107*, 2701.

(19) Che, G.; Laksmi, B. B.; Martin, C. R.; Rodney, R. S.; Fisher, E. R. *Chem. Mater.* **1998**, *10*, 260.

(20) Miller, S. A.; Young, V. Y.; Martin, C. R. *J. Am. Chem. Soc.* **2001**, *123*, 12335.

(21) Lee, J. S.; Gu, G. H.; Kim, H.; Jeong, K. S. Bae, J.; Suh, J. S. *Chem. Mater.* **2001**, *13*, 2387.

(22) Jeong, S. H.; Lee, O. J.; Oh, S. H.; Park, C. G.; Lee, K. H. *Chem. Mater.* **2002**, *14*, 1859.

(23) Yang, Q.; Xu, W.; Tomita, A.; Kyotani, T. *J. Am. Chem. Soc.* **2005**, *127*, 8956.

(24) Wang, L. S.; Lee, C. Y.; Chiu, H. T. *Chem. Commun.* **2003**, 1964.

(25) Peter, K.; Vollhardt, C.; Schore, N. E. *Organic Chemistry*, 3rd Edition: Freeman Press, New York, **1998**, p325-p326.

(26) Mckee, G. S. B.; Vecchio, K. S. *J. Phys. Chem. B* **2006**, *110*, 1179.

(27) Gregg, S. J.; Sing, K. S. W. *Adsorption, Surface Area, and Porosity*, Academic Press, London, **1982**: Chapter 3.

(28) Polarz, S.; Smarsly, B.; Schattka, J. H. *Chem. Mater.* **2002**, *14*, 2940.

(29) Shiraishi, S.; Kurihara, H.; Tsubota, H.; Oya, A.; Soneda, Y.; Yamada, Y. *Electrochem. Solid-StateLett.* **2001**, *4*, A5.

(30) Foley, H. C. *Microporous Mater.* **1995**, *4*, 407.

(31) Weast, R. C. *CRC Handbook of Chemistry and Physics*, 1st Student ed. Boca Raton FL: CRC Press, **1988**.

(32) Iijima, S. *Nature* **1991**, *354*, 56.

(33) Iijima, S.; Ichihashi, T. *Nature* **1993**, *363*, 603.

(34) Ge, J. J.; Hou, H.; Li, Q.; Graham, M. J.; Greiner, A.; Reneker, D. H.; Harris, F. W.; Cheng, S. Z. D. *J. Am. Chem. Soc.* **2004**, *126*, 15754.

(35) Zhang, W. D.; Shen, L.; Phang, I. Y.; Liu, T. *Macromolecules* **2004**, *37*, 256.